1 Introduction

In the field of spin electronics (spintronics) the spin of the electron is used as a further degree of freedom. The ongoing interest in spintronic devices is fueled by the predicted velocity of operation and the enhanced functionality. Spin related phenomena like the giant magnetoresistance [Bai88, Bin89], the tunneling magnetoresistance [Jul75, Moo95], and the anisotropic magnetoresistance [Rij95, Rij97, Ste04] have already gained industrial success and are used in hard disk read heads, magnetic random access memories, and in magnetic field sensors.

The most prominent spintronic device is the spin transistor suggested by Datta and Das [Dat90]. Recently, this device has been patented in the United States of America by Saito et al. and has been assigned to Toshiba [Sai05]. Two ferromagnetic electrodes used as spin injector and spin detector are separated by a semiconductor with a two-dimensional electron gas (2DEG). Once injected into the 2DEG the spin-polarized current can be controlled with a gate electrode via the Rashba spin-orbit interaction [Ras60, Byc84]. Towards the realization of the spin transistor, three main obstacles have to be overcome, namely, the spin injection, the spin control and the spin detection. Recent experiments have shown the tunability of the spin-orbit interaction without changing the charge carrier density [Gru00, Sch05]. For these experiments semiconductor heterostructures with an ingrown back-gate and a conducting $InAs/In_{0.75}Ga_{0.25}As$ channel have been used. Spin injection into semiconductors has been proven in experiments with optical detection of the spin polarization. The circular polarized light of an integrated light-emitting diode has been used as a measure for the spin-injection rate [Fie99]. In later experiments either Schottky barriers [Zhu01, Ram02, Han02] or oxide tunnel barriers [Mot02] have been used to increase the spin-injection efficiency from a ferromagnetic electrode into a semiconductor. The quest for electrical spin detection in semiconductors or in normal metals is still in its infancy. Only in a very limited number of experiments with all-metal hybrid systems spin detection has been proven successfully [Jed02, Kim05]. In a theoretical work it has been shown that the spin-injection efficiency is poor unless the spin polarization of the electrodes is 100 % [Sch00]. The so-called Heusler alloys are promising candidates for electrode materials with high spin polarization [vO05]. Another approach towards increased spin-injection rates is the implementation of oxide tunnel barriers at the interfaces as in the optical experiments. The increase is predicted by a theory for the diffusive transport regime [Ras02].

The present work focuses on all-metal spin-valve devices consisting of two ferromagnetic permalloy electrodes and an interconnecting aluminum strip. The micromagnetic behavior of the electrodes has been investigated and optimized with a magnetic-force microscope. Transport measurements of spin-valve devices with clean interfaces have been performed at liquid helium temperatures. Three different contributions to the magnetoresistance of the entire device have been identified, namely, the anisotropic magnetoresistance, the local Hall effect, and the spin-valve ef-

fect. Aluminum oxide tunnel barriers have been prepared and characterized in non-magnetic tunnel junctions as groundwork for future experiments. These will investigate the electrical spin detection in normal metals and in semiconductors of hybrid spin-valve devices with integrated tunnel barriers.

This thesis is organized as follows: the second chapter introduces the theoretical background of tunnel barriers, anisotropic magnetoresistance, and spin injection in the diffusive transport regime. In chapter 3, the measurement techniques and the preparation of the tunnel junctions and the spin-valve devices are described. Chapter 4 presents the results of the tunnel junctions. The micromagnetic behavior of permalloy electrodes and of permalloy rings is discussed in chapter 5. Then, chapter 6 shows the transport measurements of the spin-valve devices and an outlook on future experiments is given. The conclusions of this thesis are presented in chapter 7.

2 Theoretical background

In this chapter an introduction to the theoretical background of the experiments performed during this thesis is given. First the transport of electrons through thin tunnel barriers is described. Then the mechanism of the anisotropic magnetoresistance in ferromagnetic materials is sketched. Finally the theory of spin injection and detection in ferromagnet/normal metal hybrid devices in the diffusive regime is presented.

2.1 Tunnel barriers

Two metallic electrodes are assumed to be separated by a thin tunnel barrier. In the classical understanding of charge transport a current flow is inhibited due to a potential barrier. This barrier is higher than the Fermi energies of both electrodes. With their pioneering experiments Fisher and Giaever have proven that a current flows due to the quantum mechanical tunnel effect [Fis61]. The Nobel Prize in Physics 1973 has been awarded one quarter each to Esaki and Giaever and one half to Josephson for their discoveries of tunneling phenomena in solids.

The transition probability per time of an electron from the electrode a into the electrode b for a given transverse momentum k_t and total energy E can be written as

$$P_{ab}(E,V) = \frac{2\pi}{\hbar}|M_{ab}(E)|^2\rho_b(E-eV)f_a(E)[1-f_b(E-eV)]. \tag{2.1}$$

$M_{ab}(E)$ is the matrix element for the transition, $\rho_b(E)$ is the density of states in electrode b, $f(E)$ is the Fermi distribution function, and V is the bias voltage applied across the tunnel barrier [Har61]. The integral over all states for a fixed transverse momentum k_t and the sum over all k_t multiplied by a factor 2 for both spin directions and by the elementary charge e results in the current density from electrode a to electrode b:

$$j_{a\rightarrow b}(V) = \frac{4\pi e}{\hbar}\sum_{k_t}\int_{-\infty}^{\infty}|M_{ab}(E)|^2\rho_a(E)\rho_b(E-eV)f_a(E)[1-f_b(E-eV)]dE. \tag{2.2}$$

The current density $j_{b\rightarrow a}$ for the inverse process, i.e., tunneling from electrode b to electrode a, equals $j_{a\rightarrow b}$ except that $f_a(E)$ and $f_b(E-eV)$ are interchanged. The difference leads to the total current density through the tunnel barrier:

$$j(V) = j_{a\rightarrow b} - j_{b\rightarrow a} = \frac{4\pi e}{\hbar}\sum_{k_t}\int_{-\infty}^{\infty}|M_{ab}(E)|^2\rho_a(E)\rho_b(E-eV)[f_a(E)-f_b(E-eV)]dE. \tag{2.3}$$

Solving this integral is the main obstacle in finding a handy expression for the description of the current through tunnel barriers. In the following, two solutions derived by different approaches from Simmons [Sim63] and Brinkman et al. [Bri70] are presented.
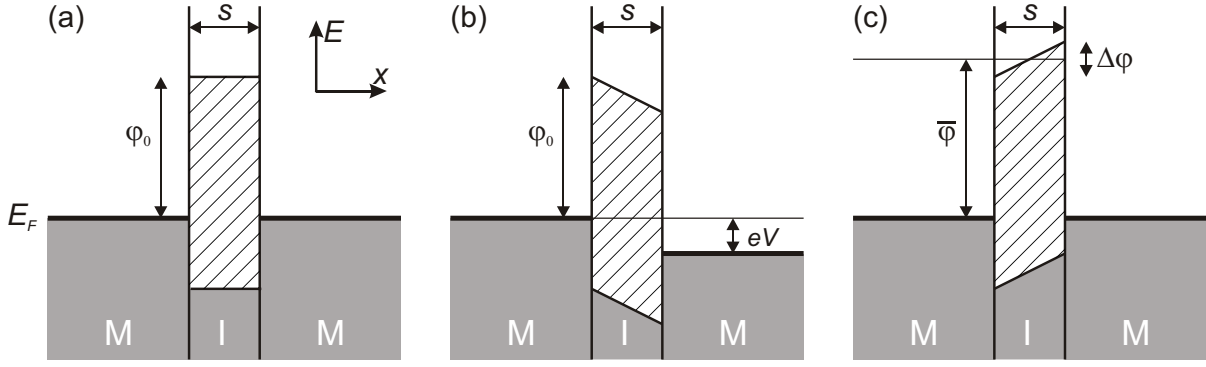
Fig. 2.1: (a) Sketch of a rectangular tunnel barrier (I) of thickness s between two metallic electrodes (M). The Fermi energy E_F in the electrodes lies in the band gap of the insulator (hatched). The barrier height φ_0 is the difference between E_F and the upper edge of the band gap of the insulator. (b) A bias voltage V is applied to the tunnel barrier. (c) Sketch of a trapezoidal barrier at zero bias. $\bar{\varphi}$ is the average barrier height and $\Delta\varphi$ is the barrier asymmetry. (a) and (b) belong to Simmons's theory and (c) to Brinkman's theory.

With the assumption of a rectangular barrier of thickness s, see Fig. 2.1(a) and (b), Simmons has found the current-voltage characteristic for intermediate voltages, i.e., the applied voltage V multiplied by e has to be smaller than the barrier height φ_0:

$$I(V) = \frac{eA}{2\pi h s^2}\left(\varphi_0 - \frac{eV}{2}\right)exp\left(-\alpha s\sqrt{\varphi_0 - \frac{eV}{2}}\right)$$
$$- \frac{eA}{2\pi h s^2}\left(\varphi_0 + \frac{eV}{2}\right)exp\left(-\alpha s\sqrt{\varphi_0 + \frac{eV}{2}}\right). \tag{2.4}$$

A is the cross-sectional area of the tunnel contact, h is Planck's constant, m is the mass of the electron, and the constant α is defined as $\alpha = 4\pi\sqrt{2m}/h$. The opposite signs of the two terms on the right side originate from the bidirectional tunneling.

Brinkman et al. have assumed trapezoidal barriers, see Fig. 2.1(c). They have calculated the tunneling current numerically and have found a parabolic dependency between the differential conductivity $dG(V)$ and the applied bias voltage for low voltages ($\lesssim 0.4\,V$):

$$\frac{dG(V)}{G(0)} = 1 - \left(\frac{C\Delta\varphi}{16\bar{\varphi}^{\frac{3}{2}}}\right)eV + \left(\frac{9}{128}\frac{C^2}{\bar{\varphi}}\right)(eV)^2 \tag{2.5}$$

$$\text{with} \quad C = \frac{4s\sqrt{2m}}{3\hbar}$$

$$\text{and} \quad G(0) = \frac{e^2A\sqrt{2m\bar{\varphi}}}{h^2 s}\exp\left(-\frac{2s}{\hbar}\sqrt{2m\bar{\varphi}}\right).$$

$\Delta\varphi$ is the asymmetry of the barrier, $\bar{\varphi}$ is the average barrier height, and $G(0)$ is the differential conductivity at zero bias. Figure 2.2(a) shows the well known shape of the tunneling current versus the applied bias voltage for an exemplary set of parameters $A = 8\times8\,\mu m^2$, $s = 1$ nm and
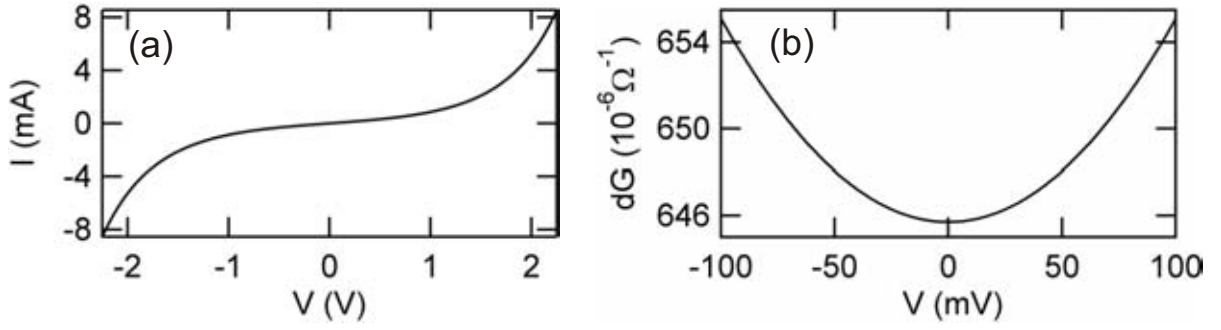
Fig. 2.2: (a) Current-voltage dependency of a tunnel barrier calculated with Eq. 2.4. The parameters used are the cross-sectional area $A = 8 \times 8\,\mu m^2$, the thickness $s = 1\,nm$ and the barrier height $\varphi_0 = 2.25\,eV$. In (b) the differential conductivity calculated with Eq. 2.5 is plotted versus the bias voltage with the same parameters (average barrier height $\bar{\varphi} = \varphi_0$) as in (a) and a barrier asymmetry $\Delta\varphi = 0$.

$\varphi_0 = 2.25\,eV$ calculated with Eq. 2.4. The differential conductivity calculated with Eq. 2.5 with the same parameters ($\bar{\varphi} = \varphi_0$) and $\Delta\varphi = 0$ is plotted in Fig. 2.2(b). The equation from Brinkman et al. is more convenient for a fit of the experimental data for two reasons. First a possible barrier asymmetry is considered in contrast to Simmons's equation. This is necessary to fit data which is asymmetric to the origin. Secondly, there are more advanced fit algorithms for parabolas leading to more reliable fit parameters. The characteristic parameters of a tunnel barrier are obtained from the coefficients of the fit of the differential conductivity as follows. The parabolic fit of the experimental data yields the coefficients $K_0(\bar{\varphi},s)$, $K_1(\bar{\varphi},\Delta\varphi,s)$, and $K_2(\bar{\varphi},s)$:

$$dG(V) = \frac{dI}{dV} = K_0(\bar{\varphi},s) + K_1(\bar{\varphi},\Delta\varphi,s)V + K_2(\bar{\varphi},s)V^2. \tag{2.6}$$

With the following equations these coefficients produce the average height, the thickness, and the asymmetry of the tunnel barrier:

$$\bar{\varphi} = \frac{e}{4}\sqrt{\frac{K_0}{2K_2}}\left|ln\left(\sqrt{K_0 K_2}\frac{h^3}{\sqrt{2}e^3 m\pi A}\right)\right|,$$

$$s = \frac{2\hbar}{e}\sqrt{\frac{K_2}{K_0}\frac{\bar{\varphi}}{m}}, \tag{2.7}$$

$$\Delta\varphi = -\frac{K_1}{K_0}\frac{12\hbar\bar{\varphi}^{\frac{3}{2}}}{\sqrt{2m}es}.$$

2.2 Anisotropic magnetoresistance

The anisotropic magnetoresistance (AMR) occurs in ferromagnetic materials and their alloys. Ferromagnetism originates from the spin imbalance of the spin-up and spin-down electrons. In the 3d-transition metals, the 4s-electrons can be assumed as free charge carriers and contribute mainly to the conductivity of these metals. The 3d-electrons can be considered as more localized to the

nuclei [Zen51a, Zen51b]. Due to the exchange energy the density of states of the spin-up electrons ($N_\uparrow$) is shifted downwards and the density of states of the spin-down electrons ($N_\downarrow$) is shifted upwards. Therefore more spin-up electrons are present resulting in a magnetization M in the absence of an external magnetic field and for temperatures below the Curie temperature:

$$M = g\frac{\mu_B}{V}(N_\uparrow - N_\downarrow). \tag{2.8}$$

g is the electron g-factor, μ_B is the Bohr magneton and V is the volume of the sample.

The AMR originates from scattering of the 4s-electrons at atomic orbitals. The scattering is more pronounced when the velocity vector and the local magnetization vector are parallel. The overall resistance of a sample which consists of a single domain is

$$R = R_\perp + \Delta R_{AMR}\cos^2(\theta). \tag{2.9}$$

$R_\perp$ is the resistance with the current density vector and the magnetization vector aligned perpendicular, ΔR_{AMR} is the maximum resistance change, and θ is the angle between the current density vector and the magnetization vector. The resistance in the parallel case ($\theta = 0$) is $R_\parallel = R_\perp + \Delta R_{AMR}$. For a detailed description of the AMR see [Rij95, Rij97, Ste04, Bol05].

2.3 Spin injection

In the diffusive transport model a current flowing from a ferromagnet (F) into a normal metal (N) creates a spin polarization in the normal metal. A sketch of a F/N interface is depicted in Fig. 2.3(a). Because of different conductivities of spin-up and spin-down electrons in the ferromagnet, the chemical potentials of both kinds of charge carriers are split up at the interface. Therefore the spin polarization of a ferromagnet can be partly transferred into a normal metal within the spin-relaxation length λ_N of the normal metal [vS87]. With a F/N/F structure (Fig. 2.3(d)) both, electrical spin injection and detection, can be realized in a single device if the length of the normal metal is in the order of λ_N.

F/N interface

The spin-relaxation length of the electrons is assumed to be much longer than their mean free path. Then the electron transport can be described in a two-current model in which the spin-up and spin-down electrons conduct independently. Therefore, one can define two different current densities $j_{\uparrow,\downarrow}$ and conductivities $\sigma_{\uparrow,\downarrow}$. By using Ohm's law the gradients of the chemical potentials of the spin-up and spin-down electrons are

$$\frac{\partial \mu_{\uparrow,\downarrow}}{\partial x}(x) = -\frac{e}{\sigma_{\uparrow,\downarrow}}j_{\uparrow,\downarrow}(x). \tag{2.10}$$

In this particular consideration we assume the charge transport to be only in x-direction. The density of states at the Fermi energy can be written as $\rho_{\uparrow,\downarrow} = \partial n_{\uparrow,\downarrow}(x)/\partial \mu_{\uparrow,\downarrow}(x)$ for small deviations
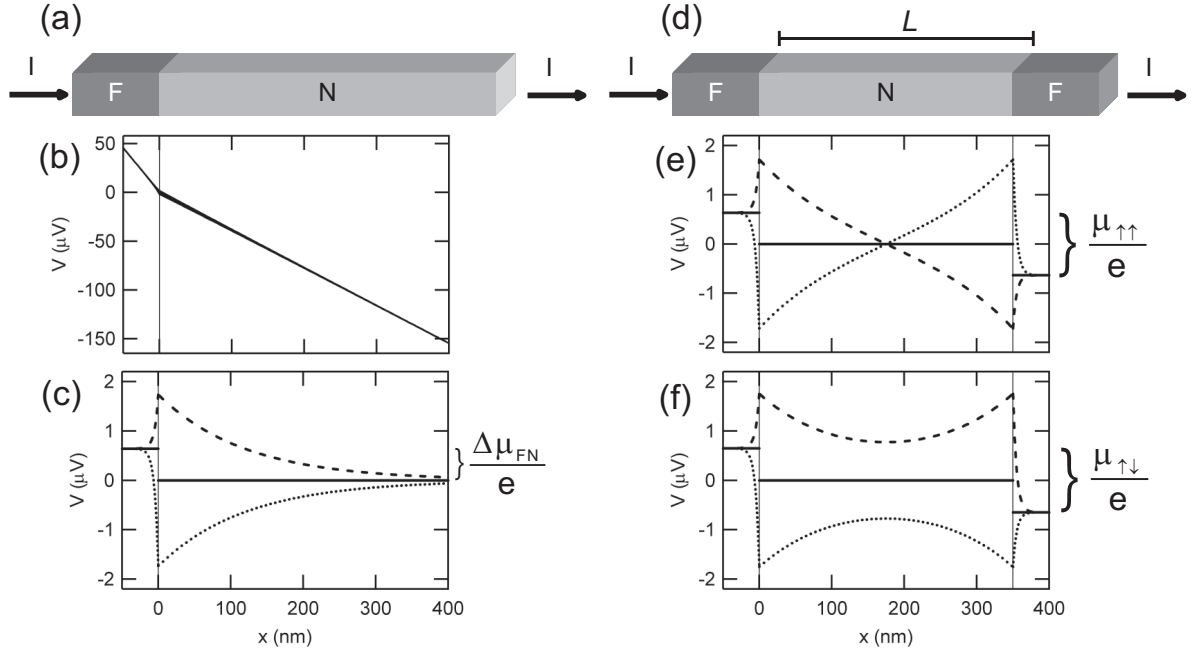
Fig. 2.3: (a) Sketch of a F/N interface. The spatial dependencies of the chemical potentials of the spin-up (dashed lines) and spin-down electrons (dotted lines), converted to voltages, are depicted in (b). Plotting the course of the chemical potentials without the linear parts of the solution the splitting of the chemical potentials become apparent in (c). The solid lines denote the resulting average chemical potentials. The interface is located at $x = 0$. (d) Sketch of a F/N/F device. In (e) and (f) the chemical potentials without the dominant linear parts are plotted for the parallel and the antiparallel configuration of the magnetizations of the ferromagnetic electrodes. The F/N interfaces are at $x = 0$ and $x = 350$ nm.

of the chemical potential from the Fermi energy. $n(x)$ is the non-equilibrium part of the particle density. Integration yields

$$\mu_{\uparrow,\downarrow}(x) = \frac{n_{\uparrow,\downarrow}(x)}{\rho_{\uparrow,\downarrow}} + \mu_0(x) \tag{2.11}$$

with $\mu_0(x)$ as the chemical potential in equilibrium. The spin polarization of the bulk current is defined as

$$\alpha = \frac{j_\uparrow - j_\downarrow}{j_\uparrow + j_\downarrow} \tag{2.12}$$

which, regarding the boundary condition of charge conservation $j = j_\uparrow + j_\downarrow$, equals the expressions $j_{\uparrow,\downarrow} = (1 \pm \alpha)j/2$. Note that these expressions are only valid in the bulk. In bulk materials the chemical potentials $\mu_\uparrow$ and $\mu_\downarrow$ equal each other and lead to the generally valid conductivities of the spin-up and spin-down electrons $\sigma_{\uparrow,\downarrow} = (1 \pm \alpha)\sigma/2$. Obviously the spin polarization of the bulk current in the normal metal is zero ($\alpha_N = 0$) and thus spin-up and spin-down electrons contribute to the total conductivity one half each. The electron transport is in the diffusive regime. Combining Fick's law and Eq. 2.10 gives a correlation between the conductivity and the diffusion constant D:

$$\sigma_{\uparrow,\downarrow} = e^2 \rho_{\uparrow,\downarrow} D_{\uparrow,\downarrow}, \quad \text{with} \quad D_{\uparrow,\downarrow} = \frac{1}{3} v_{F\uparrow,\downarrow} l_{\uparrow,\downarrow}, \tag{2.13}$$

where v_F is the Fermi velocity and l is the mean free path of the electrons. Finally the particle conservation has to be regarded:

$$\frac{\partial j_\uparrow(x)}{\partial x} = -\frac{en_\uparrow(x)}{\tau_{\uparrow\downarrow}} + \frac{en_\downarrow(x)}{\tau_{\downarrow\uparrow}} = -\frac{\partial j_\downarrow(x)}{\partial x}. \tag{2.14}$$

$\tau_{\uparrow\downarrow}^{-1}$ is the spin-flip rate from spin-up to spin-down states and $\tau_{\downarrow\uparrow}^{-1}$ is the rate vice versa. These are connected with the density of states at the Fermi energy via

$$\frac{\rho_\uparrow}{\tau_{\uparrow\downarrow}} = \frac{\rho_\downarrow}{\tau_{\downarrow\uparrow}}, \tag{2.15}$$

i.e., in equilibrium no net spin flip takes place. Combining Eqs. 2.10, 2.11, and 2.13 to 2.15 the diffusion equation for the splitting of the chemical potentials is obtained:

$$\frac{(\mu_\uparrow - \mu_\downarrow)}{\tau_{F,N}} = D_{F,N}\frac{\partial^2(\mu_\uparrow - \mu_\downarrow)}{\partial x^2}. \tag{2.16}$$

The diffusion constant $D = (1+\alpha)D_\downarrow/2 + (1-\alpha)D_\uparrow/2$ is a weighted average of the diffusion constants of the spin-up and spin-down electrons and τ_{sf}^{-1} is the sum of the spin flip rates $\tau_{\uparrow\downarrow}^{-1}$ and $\tau_{\downarrow\uparrow}^{-1}$. The spin-relaxation length is defined as $\lambda = \sqrt{D\tau_{sf}}$. The general solution of the diffusion equation is:

$$\mu_\uparrow(x) = A_{F,N} + B_{F,N}x + \frac{C_{F,N}}{\sigma_{(F,N)\uparrow}}\exp\left(-\frac{x}{\lambda_{F,N}}\right) + \frac{D_{F,N}}{\sigma_{(F,N)\uparrow}}\exp\left(\frac{x}{\lambda_{F,N}}\right) \tag{2.17}$$

$$\mu_\downarrow(x) = A_{F,N} + B_{F,N}x - \frac{C_{F,N}}{\sigma_{(F,N)\downarrow}}\exp\left(-\frac{x}{\lambda_{F,N}}\right) - \frac{D_{F,N}}{\sigma_{(F,N)\downarrow}}\exp\left(\frac{x}{\lambda_{F,N}}\right). \tag{2.18}$$

The coefficients $A_{F,N}$, $B_{F,N}$, $C_{F,N}$, and $D_{F,N}$ have to be determined in the ferromagnet (index F) and in the normal metal (index N). Therefore, the equality of $\mu_\uparrow$ and $\mu_\downarrow$ far away from the interface and the continuity of both chemical potentials and current densities at the interface have to be regarded as boundary conditions. For convenience one defines

$$R_N = \frac{\lambda_N}{\sigma_N} \quad \text{and} \quad R_F = \frac{\lambda_F}{(1-\alpha_F^2)\sigma_F}. \tag{2.19}$$

For a F/N interface located at $x = 0$ the particular solution in the ferromagnetic region ($x < 0$) is

$$\mu_\uparrow(x) = A_N + \frac{\alpha_F^2 R_N R_F e j}{R_N + R_F} - \frac{ej}{\sigma_F}x + \frac{\alpha_F(1-\alpha_F)R_N R_F e j}{R_N + R_F}\exp\left(\frac{x}{\lambda_F}\right) \tag{2.20}$$

$$\mu_\downarrow(x) = A_N + \frac{\alpha_F^2 R_N R_F e j}{R_N + R_F} - \frac{ej}{\sigma_F}x - \frac{\alpha_F(1+\alpha_F)R_N R_F e j}{R_N + R_F}\exp\left(\frac{x}{\lambda_F}\right) \tag{2.21}$$

and in the normal metal region ($x \geq 0$)

$$\mu_\uparrow(x) = A_N - \frac{ej}{\sigma_N}x + \frac{\alpha_F R_N R_F e j}{R_N + R_F}\exp\left(-\frac{x}{\lambda_N}\right) \tag{2.22}$$

$$\mu_\downarrow(x) = A_N - \frac{ej}{\sigma_N}x - \frac{\alpha_F R_N R_F e j}{R_N + R_F}\exp\left(-\frac{x}{\lambda_N}\right). \tag{2.23}$$

The parameter A_N is open and can be set to zero. Figure 2.3(a) shows a sketch of a F/N interface. The chemical potentials for a typical set of parameters ($\alpha_F = 0.37$, $\sigma_F = 3.7 \times 10^6 \, \Omega^{-1}\text{m}^{-1}$, $\sigma_N = 8.6 \times 10^6 \, \Omega^{-1}\text{m}^{-1}$, $\lambda_F = 5\,\text{nm}$, $\lambda_N = 120\,\text{nm}$, and $j = 50\,\mu\text{A}/(25\,\text{nm} \times 600\,\text{nm})$) are plotted in Fig. 2.3(b) and (c). For direct comparison with the experimental values the chemical potentials are converted to voltages. In Fig. 2.3(b) the splitting of the chemical potentials can hardly be resolved because of the dominant linear parts of $\mu_\uparrow$ and $\mu_\downarrow$ generated by the spin-independent conductivities σ_F and σ_N. Therefore these linear contributions are subtracted in Fig. 2.3(c) in order to make the spin-dependent effects visible. The average chemical potential which can be measured with voltage probes is defined as $\mu_0 = (1 + \alpha)/2 \times \mu_\uparrow + (1 - \alpha)/2 \times \mu_\downarrow$. It is depicted in Fig. 2.3(b) and (c) as solid lines. While the chemical potentials of the spin-up and the spin-down electrons have to be continuous, the average chemical potential is split up at the interface. This splitting

$$\Delta\mu_{FN} = \frac{\alpha_F^2 R_N R_F}{R_N + R_F} e j \qquad (2.24)$$

leads to a spin dependent contact resistance $\Delta R = \Delta\mu_{FN}/eI$. The spin polarization of the current at the interface is

$$P_{FN} = \frac{\alpha_F R_F}{R_N + R_F}. \qquad (2.25)$$

For the typical set of parameters mentioned above one obtains a spin polarization of 3.7 %.

F/N/F structure

In a F/N/F structure two ferromagnetic electrodes are separated by a normal metal of length L, see Fig. 2.3(d). The solution of the diffusion equation (Eq. 2.16) for this device is analogous to the solution for the F/N interface. In this case the continuity of the chemical potentials and the current densities have to be regarded at both interfaces at $x = 0$ and $x = L$. The chemical potentials $\mu_\uparrow$ and $\mu_\downarrow$ for the parallel and the antiparallel configuration of the magnetizations of the two ferromagnetic electrodes are listed in detail in Appendix A. They are sketched, converted to voltages, in Fig. 2.3(e) and (f) for the same set of parameters which have already been used for the F/N interface. The length L of the normal metal is set to 350 nm. As discussed for the F/N interface the dominant linear parts of the solution are subtracted in Fig. 2.3(e) and (f). The sum of the two splittings of the average chemical potentials at the two interfaces is

$$\mu_{\uparrow\uparrow} = \frac{2\alpha_F^2 R_N R_F \sinh(L/2\lambda_N)}{R_N \sinh(L/2\lambda_N) + R_F \cosh(L/2\lambda_N)} e j \qquad (2.26)$$

for the case of parallel orientation of the magnetizations and

$$\mu_{\uparrow\downarrow} = \frac{2\alpha_F^2 R_N R_F \cosh(L/2\lambda_N)}{R_N \cosh(L/2\lambda_N) + R_F \sinh(L/2\lambda_N)} e j \qquad (2.27)$$

for the antiparallel case. As the linear parts of the average chemical potential are spin independent and thus do not change when the magnetizations of the ferromagnetic electrodes are changed the